Paper:
Yang, F., Zuo, W., Liu, H., Song, J., Liu, H., Li, J. & Jain, S. (2019). Ion-migration and carrier-recombination inhibition by the cation- interaction in planar perovskite solar cells. *Organic Electronics*, 105387
http://dx.doi.org/10.1016/j.orgel.2019.105387

Journal Pre-proof

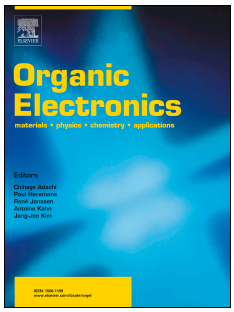

Ion-migration and carrier-recombination inhibition by the cation-π interaction in planar perovskite solar cells

Feng Yang, Weiwei Zuo, Hui Liu, Jian Song, Hairui Liu, Junming Li, Sagar M. Jain

PII: S1566-1199(19)30406-9

DOI: https://doi.org/10.1016/j.orgel.2019.105387

Reference: ORGELE 105387

To appear in: *Organic Electronics*

Received Date: 29 May 2019

Revised Date: 2 July 2019

Accepted Date: 30 July 2019

Please cite this article as: F. Yang, W. Zuo, H. Liu, J. Song, H. Liu, J. Li, S.M. Jain, Ion-migration and carrier-recombination inhibition by the cation-π interaction in planar perovskite solar cells, *Organic Electronics* (2019), doi: https://doi.org/10.1016/j.orgel.2019.105387.

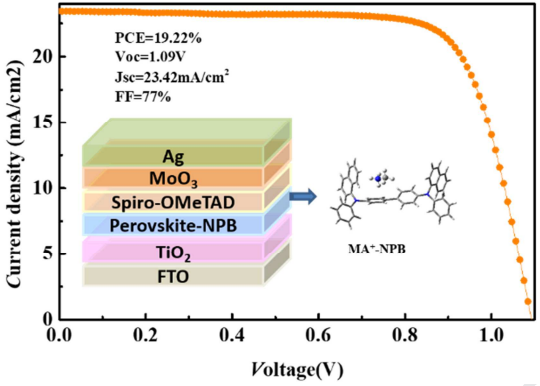

The *J-V* curves of the champion PSCs by introduced NPB into $MAPbI_3$

The high performance devices were realized by introducing small molecule N,N'-bis(naphthalen-1-yl)-N,N'+-bis(phenyl)benzidine (NPB) in $MAPbI_3$ perovskite layer. A high efficiency of 19.22% was achieved based on NPB modified $MAPbI_3$ with improved stability and suppressed hysteresis, which can be attributed to cation-π interaction between NPB and MA^+. The introduced NPB not only reduce intrinsic defects in perovskite films, enhance the crystallization and passivate the perovskites films, which is benefit to improve the stability of perovskite film and improved the efficiency of planar perovskite solar cells.

Cation-π Interaction in Planar Perovskite Solar Cells

Feng Yang[a], Weiwei Zuo[b], Hui Liu[a], Jian Song[a], Hairui Liu[a*], Junming Li[c*] and Sagar M. Jain[d*]

a, College of Physics and Materials Science, Henan Normal University, 453007 Xinxiang China
b, School of Materials Science and Engineering, Zhengzhou University, 450001 Zhengzhou China.
c, School of Physics and Electronic Engineering, Linyi University, Linyi China.
d, SPECIFIC, College of Engineering, Swansea University Bay Campus, Fabian Way, SA1 8EN Swansea, United Kingdom

Corresponding author: liuhairui1@126.com; s.m.jain@swansea.ac.uk;

Abstract: In organic-inorganic hybrid perovskite solar cells, migration of intrinsic ions (e.g., MA^+, Pb^{2+}, I^-) have a significant impact on the current-voltage hysteresis and stability of devices. Here, N, N'-diphenyl-1, 1'-biphenyl-4, 4'-diamine (NPB) was introduced into $MAPbI_3$ perovskite layer to facilitate the stability of perovskite film and improved the efficiency of planar perovskite solar cells (PSCs). The results suggest that migration of intrinsic ions are inhibited effectively by cation-π interaction between NPB and MA^+, and lead to reduce intrinsic defects in perovskite films, which is benefit for the stability of devices. Lewis basicity of NPB enhances the crystallization, passivates the perovskites films and addresses the issue of low electron extraction efficiency. Consequently, solar cells made using NPB modified $MAPbI_3$ resulted hysteresis-free, enhanced power conversion efficiency of 19.22% with improved stability.

Keywords: Perovskite Solar Cells; Migration of intrinsic ions; Cation-π Interaction

their excellent optoelectronic performance [1,2], large absorption coefficient [3,4], high carrier mobility [5], large diffusion length [6,7], and tunable flexibility in bandgap [8-10]. In recent years, organic–inorganic hybrid perovskite solar cells (PSCs) have emerged as a very promising alternative for next-generation solar cell technology and the power conversion efficiency (PCE) kept rising from 3.8% in 2009 years to 23.2% [11-13]. Given the impressive gains in PCE, it is natural that long time stability becomes the main research topic in the community. So much intrinsic defects produced during annealing or light irradiation, such as ionic migration and vacancy of the ions, inevitably result in instability of perovskite [14-16]. The ion migration problem has been considered as the one of main reasons for causing instability and degradation in the perovskite solar cells.

Several of researchers attempt to suppress the ion-migration by all kinds of experimental and theoretical methods [17-20]. In fact, there are two main mobile ions in the organic-inorganic perovskites (OIPs), the organic cation and halide ions [21,22]. In addition, poling field would result in the organic redistribution, which would affect the chemical and electric equilibrium of solar cell devices [23]. Thus, inhibiting organic cation migration could enhance the electrical transport properties and stability of the OIPs device efficiently.

Cation–π interaction is a type of electrostatic attraction between cation and large π surface of benzene and other aromatic [24]. It presents astonishing stabilization with

by mixing aromatic NPB into perovskite films, this assist during the film-forming process to restrict the migration of organic cations. Thus, by fine tuning the concentration of NPB in $MAPbI_3$ leads to suppressing cation mobility and hysteresis in solar cells that resulted into the improved performance and stability of PSCs.

2. Experiment

The glass/FTO substrate of 25×25 mm^2 square shape was sequentially washed with isopropanol, acetone, alcohol and distilled water. The sheet resistance of FTO (the thicknesses ~250 nm) used here is about 14 Ω. For TiO_2 nanoparticles films, $TiCl_4$ (4.5 ml) solution is instilled into 200 ml distilled water ice cube. Sixty minutes later, this $TiCl_4$ solution is poured into culture dish in which there lies washed glass/FTO substrate and then annealed in drying oven at 70 □ for 60 min. After 30 min ozone treatment for the TiO_2 film (electron transport layer), the perovskite film was spin-coated onto the TiO_2 layer at 1000 rpm/10 s and then 4000 rpm/40 s using the mixed solution of chlorobenzene and NPB as anti-solvent. Perovskite-NPB graded heterojunction would be obtained. This precursor film was annealed at 100 □ for 10 min in nitrogen glove box. After annealing, HTLs (Spiro-OMeTAD) in chlorobenzene solution was coated onto the perovskite layer at 5000 rpm/30 s. Finally, MoO_3 layer (10 nm) and Ag electrode (150 nm) was evaporated in vacuum chamber under vacuum at 2×10^{-6} Torr.

Current density–voltage characteristics of perovskite solar cells were performed

measurement was carried out by a system combining a xenon lamp, a monochromator, a chopper, and a lock-in amplifier together with a calibrated silicon photodetector. The absorbance of the HTLs films was measured with an UV-vis spectrophotometer (PerkinElmer Lambda 750). The surface morphology of a typical sample was characterized by SEM SUPRA™ 40. Steady-state PL measurements were acquired using Edinburgh Instruments FLS920 fluorescence spectrometer with a 532 nm pulsed laser as excitation source at the room temperature.

3. Results and discussion:

Fig. 1(a) shows the device configuration of planar heterojunction perovskite solar cells. The micro-molecular organics N,N′ -diphenyl-1,1′ -biphenyl-4,4′ -diamine (NPB) (the molecular structure of NPB is shown in Fig. 1(b)) is introduced into the perovskite absorber layer. This introduced NPB-$MAPbI_3$ perovskite employed into the FTO/TiO_2/$MAPbI_3$-NPB/Spiro-OMeTAD/Ag solar cell architecture. NPB often used as the hole transporting layer (HTL) in PSCs due to its matching bandgap between the HOMO level (5.4 eV) and the VB edge of the $MAPbI_3$. When NPB introduced in $MAPbI_3$, cation-π interaction between electron-rich π system and adjacent MA^+ cation will form by noncovalent forces when introduce aromatic NPB into $MAPbI_3$ [24]. To make sure formation of cation-π interaction, the main structure parameters and the optimized geometry active site were calculated and was chosen by density functional

initial position points were optimized under B3LYP-D3/6-311G (d.p) level with dispersion corrections. Frequency calculations were carried out to ensure that the conformations obtained are stable points. Single point energy calculations with the correction of basis set superposition error (BSSE) were performed to estimate the interaction energy. Two most stable cation-π interaction positions (labeled locus 3# and locus 6#, respectively) shown in Fig. 1(c) and (d), which have no imaginary frequency and the lowest energies, were selected from the six possible positive points. According to the results, the stable molecular structures of MA^+-NPB have two N-H bonds of MA^+ cations toward NPB with the bond lengths of 1.04 Å, which hook the central tetracene for interactions of $\sigma_{N–H-\pi NPB}$. Moreover, these two N-H bonds are a little longer than that of the other N-H bond pointing away from NPB (1.02 Å) (as shown in Fig. 1(c) and (d)). Different bond length reveals the interaction between NPB and perovskite materials again. In addition, the interaction between MA^+ cations and NPB has relative larger interaction energy (-35.2 kcal mol^{-1} (locus 3#) and -39.2 kcal mol^{-1} (locus 6#) in gas phase), which is remarkably stronger than that of a common cation-π interaction such as MA^+-benzene (-18.8 kcal mol^{-1} in gas phase). It is reported that cations are always strongly attracted to the π face of benzene and other aromatic structures [26]. Therefore, such strong interaction could be attributed to the synergetic effect of multiple off-axis cation-π interactions, leading to the mobile organic cations MA^+ anchored firmly by NPB [27].

turns to the hydrogen atom of NPB at the edge (Figure S2). And the calculated interaction energy between I^- anion and NPB in the most stable locus is only -14.47 kcal mol^{-1} in gas phase. Summary, cation-π interaction plays the main role of the interaction between perovskite and NPB, which would benefit to the inhibition of the ion migration.

To clarify the effect of cation-π interaction on the inhibition of ion migration in the perovskite solar cells, the current-density-voltage (*J*-*V*) properties of the planar heterojunction perovskite solar cell with different concentration of NPB introduced into $MAPbI_3$ are shown in Fig. 2(a). Moreover, the corresponding average results of photovoltaic parameters are summarized in Table 1. It can be clearly seen that both the short-circuit current density J_{sc} and open-circuit voltage V_{oc} keep increasing with the increasing of NPB content. Especially, J_{sc} increases strikingly from 21.93 to 23.42 mA/cm^2. On the other hand, the filler factor FF reaches the peak point of 77% for the perovskite film introducing with 6 mg/ml NPB. Moreover, on further increasing the concentration of NPB, the value of FF begins to decrease. However, the optimum PCE of 19.22% is obtained for the $MAPbI_3$ added with 9 mg/ml NPB, although the FF is slightly decline compared to introducing 6 mg/ml NPB. This PCE is significantly higher than the control planar PSCs (17.36%). This suggests that optimum introducing of NPB can remarkably improve the electrical properties of the perovskite solar cell. Solar cell statistics of 60 devices prepared using optimized NPB

employs NPB introduced $MAPbI_3$ as absorber.

The corresponding incident photon-to-current conversion efficiency (IPCE) and the integrated J_{sc} (from IPCE curves) of device with and without NPB is characterized and compared (as shown in Fig. 2(b)). There is a wide and flat wavelength band increment of IPCE for device with NPB introducing in core absorption region from 350 nm to 700 nm spectra, the value of IPCE curve reach over 90%. This wideband enhancement means that the J_{sc} increasing of the PSC as a reason of NPB introducing that attributes to the improvement of crystallinity of the perovskite film [28]. As we known, the high crystallinity of perovskite film with lower defects will result in more efficient charge carrier generation and transport in the cation-immobilized perovskite films, which would inhibit the loss of photo-induced carriers during transfer, and then enhance the collection of photo-induced carriers in PSC. Therefore, the intrinsic reason is that the PSC introduced NPB possesses faster transport of photo-generated carriers and less recombination centers [29,30]. The integrated J_{sc} from IPCE curves also agree with the measured J_{sc} very well. In addition, the stabilized current density and PCE at the maximum power point as a function of time are also recorded. As shown in Fig. 2(c), a stabilized PCE of 18.56% with a current density of ~21.57 mA/cm^2 is obtained, showing a stable output characteristic within 300 s.

J-V hysteresis characterization gives an estimation of the charge transport and ion migration in PSCs. Device performance under reverse and forward scans with and

exhibited significant hysteresis. Meanwhile, PSCs with NPB modification present a negligible hysteresis (hysteresis index ¼ 1.0%). The suppressed negligible hysteresis PSCs indicates fewer defects at the NPB introducing perovskite interface due to better crystallinity and coverage of perovskite film on TiO_2.

OIPs has been beset by hysteresis for long time, which is caused by both scan rate and direction of the *J-V* characteristics [31]. It is widely reported that hysteresis is always attributed to the reducing built-in electric field by the changing quantities of charge accumulated at the $MAPbI_3$ interfaces, resulting in loss of photocurrent [14,32,33]. Furthermore, ion migration under external electric field is considered as causing the accumulation of mobile ions at the interfaces [34]. Therefore, ion migration plays an important role in device hysteresis behavior [35-37]. In $MAPbI_3$ based perovskite solar cell, MA^+ cation is one of the main mobile ions. Once illuminated, large number of cations would migrate freely in $MAPbI_3$ and can interfere charges, this result in notorious, noticeable *J-V* hysteresis phenomenon [37]. Thus, suppressing ion migration would govern the current-voltage hysteresis. PSCs prepared from NPB introduced $MAPbI_3$ showed hysteresis-free *J-V* curves as presented in the Fig. 2(d). Considering the fact that mobile ions contribute for hysteresis, this clearly shows that the mobile ions can be well inhibited. This can be contributed to the cation-π interaction between NPB and MA^+ as motioned earlier.

Moreover, to study the optoelectronic changes in $MAPbI_3$ film with and without

without NPB were deposited on FTO/TiO_2 film. As shown in Fig. 3(a), NPB introduced in perovskite film shows enhanced absorbance covering almost all the visible light region, which is attributed to the improved crystalline of NPB-$MAPbI_3$ films (Fig. S4). Furthermore, the steady-state photoluminescence (PL) spectra (Fig. 3(b)) and time-resolved photo-luminescence (TRPL) spectra (Fig. S5) of the perovskite film with and without NPB were employed to study the impact of NPB and MA^+ on the extraction of electrons and charge recombination in perovskite film. The steady state PL intensity of NPB-$MAPbI_3$ film is reduced than that of the pristine $MAPbI_3$ film, which is attributed better charge transport across NPB-$MAPbI_3$/TiO_2 interface.

To understand the effects of the carriers migration on interface charge transport, the Nyquist plots of the electrochemical impedance spectra (EIS) under the illumination of AM 1.5G in ambient air was performed for device with and without NPB (as shown in Fig. 3(c)). In general, the internal series resistance (R_s) in the higher frequency represents the ohmic resistance consists of the sheet resistance (R_{SHEET}) of the electrodes, the charge-transfer resistance (R_{CT}) at the interfaces between electrode and carriers transfer layer (included holes transfer layer and electrons transfer layer) and between carriers transfer layer and the perovskite layer [38,39]. Because all the samples in this experiment possess the same device structure, R_{SHEET} could be assumed to be the same. The only difference is the R_{CT} which arises

perovskite film. Most portion of NPB stayed on the upper layer of the perovskite film. As a result, the R_{CT} arises from ETL/perovskite interface were also considered as same. Therefore, impedance spectrometry could be used to investigate the electrical properties of the HTL/perovskite interfaces. Attractively, R_{CT} values of 32.85 and 105.05 kΩ were obtained by testing the devices with and without NPB into perovskite layer, respectively. Without NPB, a large R_{CT} value indicated that the large charge-transfer resistance resulted from the inferior contact at the interface with the Spiro-OMeTAD/$MAPbI_3$. While, with NPB introduced into the perovskite film, smaller R_{CT} was obtained as a result of the larger interfacial area between $MAPbI_3$ and Spiro-OMeTAD, which is benefit to the transmission of the photo-induced carriers. Therefore, it is a corroborative evidence for the higher PCE from the NPB-$MAPbI_3$ than from the pure $MAPbI_3$.

In order to understand further the NPB introducing devices can reduce the carrier recombination, dark *J-V* characteristics of the solar cell prepared with and without NPB introduced $MAPbI_3$ films measured and shown in Fig. 3d. It presents a prominent rectifying characteristic with a lower reverse leakage current and higher forward conducting current. The dark current density of the solar cell device with NPB-$MAPbI_3$ film is obviously lower than the pristine device. This obvious decreasing leakage current can be contributed to the cation-π interaction in the NPB-$MAPbI_3$. Additionally, the devices based on NPB-$MAPbI_3$ and pristine

X-ray diffraction (XRD) recorded for $MAPbI_3$ film with and without NPB. As shown in Fig. 4(a), the main diffraction peaks at 14.2° and 28.4° are assigned to the (110) and (220) planes of tetragonal crystal structure of $MAPbI_3$. The diffraction peaks of NPB-$MAPbI_3$ film became clearly enhanced, indicating that the crystallinity of perovskite films is improved. Moreover, the full widths at half maximum of the two main peaks enlarge slightly due to the formation of the bigger sized perovskite grain. Hence, NBP introduced is help to the improvement of the crystallinity and the growth of crystal grain of perovskite film. This is further confirmed from the SEM surface morphology images Fig. 4(b-f).

In the SEM experiment, we fix the optimal perovskite layer thickness of ~300 nm for all the devices to exclude the variations in optical absorption or interference effects. As shown in Fig. 4(b-f), the perovskite film without NPB has no very clear grain boundary. The heterogeneity of grain size is the other microstructure of that film. With the concentration increasing for NPB into $MAPbI_3$ film, the size of crystal grain increases slowly and the boundary becomes more distinct. However, the precipitation phase appear gradually between grain boundaries as the stoichiometry of NPB increasing over 9 mg/ml. SEM images demonstrate again that NPB introduced is favorable for perovskite crystallization, enlarge the grain and improve morphology of the perovskite film. It is reported that better crystallinity and less defect material result in less traps and mobile ions, which were beneficial for charge transporting, as well as

could lead to a reduction in collection efficiency [44]. Therefore the effective suppression of hysteresis effects is attributed to the improving morphology of the interface of perovskite/HTLs, which leads to relative high efficient charge extraction and then result in the increasing of J_{sc} and PCE.

Long-term stability is another critical characteristic for PSCs, especially the operational stability under 1 sun illumination in ambient air. To investigate the stability of devices with the NPB-$MAPbI_3$ and pristine $MAPbI_3$, we performed stability tests of PSCs without encapsulation and under identical storage conditions 1 sun illumination (illumination for one week). And their efficiency was periodically measured to check the long-term stability. All the devices exposure to ambient air in the Sample Storage Room where maintained in about 20 degree centigrade and 40% relative humidity. As shown in Fig. 5(a), the PCEs of typical PSCs with $MAPbI_3$ retained only about 24 % of their initial efficiency. However, the devices with $CH_3NH_3PbI_3$-NPB film exhibit the retention of PCE about 83 % of the initial value. The inset of Fig. 5(a) show that the NPB-$MAPbI_3$ films with larger water contact angle of 42.10° than that of pure $MAPbI_3$ (36.00°). It indicates that the NPB-$MAPbI_3$ films could prevent the water, to some extent. In addition, the XRD patterns were measured for the samples exposed in air for 48 h (~40% relative humidity) (as shown in Fig.5 (b)). As expected, an obvious new peak appeared in the XRD curve without NPB at 12.6°, indicates the decomposition of perovskite materials and the appearance

In general, the higher stability of PSCs attributed to the hydrophobic properties [35,45,46]. The water molecules in aqueous environments would combine easily with MA^+ cations of the pristine perovskite materials and neutralize the charges of the cations, which leads to the loss of MA^+ and cause the decomposition of perovskite materials [47]. However, the introduction of hydrophobic binding site comprised of aromatic rings can compete with full aqueous solvation in the binding of highly cations in $MAPbI_3$ materials, which is important for the stability of PSCs [48]. In the NPB introducing perovskite PCSs, and higher interaction energy of cation-π interaction between MA^+ in the perovskite and aromatic rings in NPB not only improves the quality of perovskite film but also induce hydrophobicity to formation stable perovskite devices.

4. Conclusions

Fine tuning of NPB in $MAPbI_3$ induce the cation-π interaction that is able to effectively suppress the migration of MA^+ in OIPs. PSCs made employing optimal quantity of NPB-introduced $MAPbI_3$ shown record hysteresis-free efficiency of 19.22%. Additionally, the introducing of NPB also improved the crystalline quality of the perovskite film that ultimately resulted into enhanced stability of solar cells prepared using NPB-$MAPbI_3$. The NPB-$MAPbI_3$ film possesses effectively transport of photo-generated carriers and less recombination centres, which mainly due to inhibition of MA^+ in perovskite. This work gives a novel methodology for suppressing the notorious hysteresis phenomenon as well improving the efficiency

There are no conflicts to declare.

Acknowledgement

This work has been supported by the National Natural Science Foundation of China (Grant No. 51502081, 11504093 and No. 11674144), the Basic Research Projects in Henan Province, China (Grant No. 122300410231). S. M. J. acknowledge Marie Curie COFUND fellowship, Welsh Assembly Government funded Ser-Cymru Solar Project, European Union's Horizon 2020 research and innovation programme under the Marie Skłodowska-Curie grant agreement No 663830 and the Natural Science Foundation of Shandong Province (Grant Nos. JQ201602 and ZR2018MA038).

Reference

[1] C. Eames, J. M. Frost, P. R. F. Barnes, B. C. ÒRegan, A. Walsh and M. S. Islam, Ionic transport in hybrid lead iodide perovskite solar cells, Nat. Commun., 6 (2015) 7497.

[2] A. Kojima, K. Teshima, Y. Shirai, T. Miyasaka, Organometal Halide Perovskites as Visible-Light Sensitizers for Photovoltaic Cells, J. Am. Chem. Soc., 131 (17) (2009) 6050–6051.

[3] G. E. Eperon, V. M. Burlakov, P. Docampo, A. Goriely and H. J. Snaith, Morphological Control for High Performance, Solution-Processed Planar Heterojunction Perovskite Solar Cells, Adv. Funct. Mater., 24 (1) (2013) 151-157.

[4] D. W. Stefaan, H. Jakub, S. J. Moon, L. Philipp, N. Bjoern, L. Martin, F. J. Haug, J. H. Yum, C. Ballif, Organometallic Halide Perovskites: Sharp Optical Absorption Edge and Its Relation to Photovoltaic Performance, J. Phys. Chem. Lett., 5 (6) (2014) 1035-1039.

[5] F. Deschler, M. Price, S. Pathak, L. E. Klintberg, D. D. Jarausch, R. Higler, S. Huttner, T. Leijtens, S. D. Stranks, H. J. Snaith, M. Atature, R. T. Phillips, R. H. Friend, High Photoluminescence Efficiency and Optically

[6] S. D. Stranks, G. E. Eperon, G. Grancini, C. Menelaou, M. J. Alcocer, T. Leijtens, L. M. Herz, A. Petrozza, H. J. Snaith, Electron-hole diffusion lengths exceeding 1 micrometer in an organometal trihalide perovskite absorber, Science, 342 (6156) (2013) 341-344.

[7] G. Xing, N. Mathews, S. Sun, S. S. Lim, Y. M. Lam, M. Gratzel, S. Mhaisalkar, T. C. Sum, Long-range balanced electron and hole-transport lengths in organic-inorganic $CH_3NH_3PbI_3$, Science, 342 (6156) (2013) 344-347.

[8] G. E. Eperon, S. D. Stranks, C. Menelaou, M. B. Johnston, L. M. Herz, Henry J. Snaith, Formamidinium lead trihalide: a broadly tunable perovskite for efficient planar heterojunction solar cells, Energ. Environ. Sci., 7 (3) (2014) 982.

[9] M. R. Filip, G. E. Eperon, H. J. Snaith, F. Giustino, Steric engineering of metal-halide perovskites with tunable optical band gaps, Nat. Commun., 5 (2014) 5757.

[10] N. K. Kumawat, A. Dey, A. Kumar, S. P. Gopinathan, K. L. Narasimhan, D. Kabra, Band Gap Tuning of $CH_{(3)}NH_{(3)}Pb(Br_{(1-x)}Cl_x)_{(3)}$ Hybrid Perovskite for Blue Electroluminescence, ACS Appl. Mater. Interfaces, 7 (24) (2015) 13119-13124.

[11] W. S. Yang, B. W. Park, E. H. Jung, N. J. Jeon, Y. C. Kim, D. U. Lee, S. S. Shin, J. Seo, E. K. Kim, J. H. Noh, S. I. Seok, Iodide management in formamidinium-lead-halide-based perovskite layers for efficient solar cells, Science, 356 (2017) 1376-1379.

[12] J. A. Christians, P. Schulz, J. S. Tinkham, S. P. Harvey, B. J. Tremolet de Villers, A. Sellinger, J. J. Berry and J. M. Luther, Tailored interfaces of unencapsulated perovskite solar cells for >1000 hour operational stability, Nat. Energy, 3 (2018) 68-74.

3 (1) (2018) 682-689.

[14] P. Calado, A. M. Telford, D. Bryant, X. Li, J. Nelson, B. C. O'Regan, P. R. Barnes, Evidence for ion migration in hybrid perovskite solar cells with minimal hysteresis, Nat. Commun, 7 (2016) 13831.

[15] R. A. Belisle, W. H. Nguyen, A. R. Bowring, P. Calado, X. Li, S.t J. C. Irvine, M. D. McGehee, P. R. F. Barnes, B. C. O'Regan, Interpretation of inverted photocurrent transients in organic lead halide perovskite solar cells: proof of the field screening by mobile ions and determination of the space charge layer widths, Energ. Environ. Sci., 10, (2017) 192.

[16] N. G. Park, M Grätzel, T. Miyasaka, K. Zhu, K. Emery, Towards stable and commercially available perovskite solar cells, Nat. Energ., 1 (11) (2016) 16152.

[17] J. S. Yun，J. Seidel，J. Kim, A. M. Soufiani, S. Huang，J. Lau, N. J. Jeon, S. I. Seok, M. A. Green, A. Ho-Baillie, Critical Role of Grain Boundaries for Ion Migration in Formamidinium and Methylammonium Lead Halide Perovskite Solar Cells, Adv. Energ. Mater., 6 (13) (2016) 1600330.

[18] Y. Lin, Y. Bai, Y. J. Fang, Q. Wang, Y. H. Deng, J. S. Huang, Suppressed Ion Migration in Low-Dimensional Perovskites, ACS Energy Lett., 2 (2017) 1571-1572.

[19] Y. Yuan, J. Huang, Ion migration in organometal trihalide perovskite and its impact on photovoltaic efficiency and stability, Accounts Chem. Res., 49 (2) (2016) 286-93.

[20] J. Haruyama, K. Sodeyama, L. Han and Y. Tateyama, First-principles study of ion diffusion in perovskite solar cell sensitizers, J. Am. Chem. Soc., 9 (39) (2015) 33802-33809.

[21] Y. X. Liu, K. Palotas, X. Yuan, T. J. Hou, H. P. Lin, Y. Y. Li and S. T. Lee, Atomistic origins of surface defects in $CH_3NH_3PbBr_3$ perovskite and their electronic structures, ACS Nano 11 (2) (2017) 2060-2065.

[23] Z. G. Xiao, Y. B. Yuan, Y. C. Shao, Q. Wang, Q. F. Dong, C. Bi, P. Sharma, A. Gruverman and J. S. Huang, Giant switchable photovoltaic effect in organometal trihalide perovskite devices, Nat. Mater., 14 (2015) 193-198.

[24] D. A. Dougherty, The cation-π interaction, Accounts Chem. Res., 46 (4) 2013 885-893.

[25] D. Wei, F. S. Ma, R. Wang, S. Y. Dou, P. Cui, H. Huang, J. Ji, E. D. Jia, X. J. Jia, S. Sajid, A. M. Elseman, L. H. Chu, Y. F. Li, B. Jiang, J. Qiao, Y. B. Yuan, M. C. Li, Ion-Migration Inhibition by the Cation-pi Interaction in Perovskite Materials for Efficient and Stable Perovskite Solar Cells, Adv. Mater., 30 (31) (2018) 1707583.

[26] D. A. Dougherty, Cation-π interactions in chemistry and biology: a new view of benzene, Phe, Tyr, and Trp, Science, 271, (1996) 163-168.

[27] M. S. Marshall, R. P. Steele, K. S. Thanthiriwatte and C. D. Sherrill, Potential Energy Curves for Cation-π Interactions: Off-Axis Configurations Are Also Attractive, J. Phys. Chem. A, 113, (2009) 13628-13632.

[28] Dixon D. S. Fung, L. F. Qiao, Wallace C. H. Choy, C. D. Wang, Wei E. I. Sha, F. X. Xie, S. L. He, Optical and electrical properties of efficiency enhanced polymer solar cells with Au nanoparticles in a PEDOT-PSS layer, J. Mater. Chem., 21 (2011) 16349.

[29] Q. Q. Lin, A. Armin, R. C. R. Nagiri, P. L. Burn, P Meredith, Electro-optics of perovskite solar cells, Nat. Photonics, 9 (2014) 106-112.

[30] J. P. Correa-Baena, M. Anaya, G. Lozano, W. Tress, K. Domanski, M. Saliba, T. Matsui, Tor J. Jacobsson, M. E. Calvo, A. Abate, M. Grätzel, H. Míguez, A. Hagfeldt, Unbroken perovskite: interplay of morphology, electro-optical properties, and ionic movement, Adv. Mater., 28 (25) (2016) 5031-5037.

[31] H. J. Snaith, A, Abate, J. M. Ball, G. E. Eperon, T. Leijtens,Noel, K. Nakita，S. D. Stranks, J. Tse-Wei Wang,

[32] B. Wu, K. W. Fu, N. Yantara, G. C. Xing, S. Y. Sun, T. C. Sum, N. Mathews, Charge accumulation and hysteresis in perovskite-based solar cells: an electro-optical analysis, Adv. Energy Mater., 5 (19) (2015) 1500829.

[33] S. van Reenen, M. Kemerink, and H. J. Snaith, Modeling anomalous hysteresis in perovskite solar cells, J. Phys. Chem. Lett., 6 (19) (2015) 3808-14.

[34] Y. Zhang, M. Z. Liu., G. E. Eperon, T. Leijtens, D. McMeekin, M. Saliba, W. Zhang, M. de Bastiani, A. M. Petrozza, L. M. Herz, M. B. Johnston, H. Lin, H. J. Snaith, Charge selective contacts, mobile ions and anomalous hysteresis in organic-inorganic perovskite solar cells, Mater. Horiz., 2 (2015) 315-322.

[35] V. Nandal, P. R. Nair, Predictive modeling of ion migration induced degradation in perovskite solar cells, ACS Nano, 11 (2017) 11505-1151.

[36] Y. Zhao, C. J. Liang, H. M. Zhang, D. Li, D. Tian, G. B. Li, X. P. Jing, W. G. Zhang, W. K. Xiao, Q. Liu, F. J. Zhang and Z. Q. He, Anomalously large interface charge in polarity-switchable photovoltaic devices: an indication of mobile ions in organic–inorganic halide perovskites, Energy Environ. Sci., 00 (2015) 1-3.

[37] H. M. Zhang, C. L. Liang, Y. Zhao, M. J. Sun, H. Liu, J. J. Liang, D. Li, F. J. Zhang and Z. Q. He, Dynamic interface charge governing the current-voltage hysteresis in perovskite solar cells, Phys. Chem. Chem. Phys., 17 (2015) 9613-9618

[38] C. Liu, K. Wang, P. P. Du, C. Yi, T. Y. Meng, X. Gong, Efficient Solution‐Processed Bulk Heterojunction Perovskite Hybrid Solar Cells, Adv. Energy Mater., 5 (12) (2015) 1402024.

[39] K. Wang, C. Liu, P. P. Du, J. Zheng and X. Gong, Bulk heterojunction perovskite hybrid solar cells with large fill factor, Energy Environ. Sci., 8 (2015) 1245-1255.

Cells, Adv. Electron. Mater., 3 (2) (2017) 1600470.

[41] F. Wu, T. Chen, X. Yue, L. N. Zhu, Enhanced photovoltaic performance and reduced hysteresis in perovskite-ICBA-based solar cells, Org. Electron., 58 (2018) 6-11.

[42] W. Nie, H. Tsai, R. Asadpour, J. C. Blancon，A. J. Neukirch, G. Gupta, J. J. Crochet, M. Chhowalla, S. Tretiak, M. A. Alam, H. L. Wang, A. D. Mohite, High-efficiency solution-processed perovskite solar cells with millimeter-scale grains, Science, 347 (6221) (2015) 522-525.

[43] M. Li, Y. G. Yang, Z. K. Wang, T. Kang, Q. Wang, S. H. Turren-Cruz, X. Y. Gao, C. Sh. Hsu, L. S. Liao, and An Abate, Perovskite Grains Embraced in a Soft Fullerene Network Make Highly Effcient Flexible Solar Cells with Superior Mechanical Stability, Adv. Mater., 31 (2019) 1901519.

[44] Y. Yuan, J. Huang, Ion migration in organometal trihalide perovskite and its impact on photovoltaic efficiency and stability, Acc. Chem. Res., 49 (2) (2016) 286-93.

[45] Y. Hou, H. Zhang, W. Chen, S. Chen, C. O. R. Quiroz, H. Azimi, A Osvet, G. J. Matt,; E. Zeira, J. Seuring, N. Kausch-Busies, W. Lövenich, C. J. Brabec, Inverted, Environmentally stable perovskite solar cell with a novel low-cost and water-free PEDOT hole-extraction layer, Adv. Energ. Mater., 5 (15) (2015) 1500543.

[46] L. L. Zheng, Y. H. Chung, Y. Z. Ma, L. P. Zhang, L. X. Xiao, Z. J. Chen, S. F. Wang, B. Qu and Q. H. Gong, A hydrophobic hole transporting oligothiophene for planar perovskite solar cells with improved stability, Chemistry Commun., 50 (2014) 11196.

[47] G. Yang, Y. Ma and W. H. Xing, The effect of cation-π interactions in electrolyte/organic nanofiltration systems, Chinese J. Chem. Eng., 24 (2016) 345-352.

[48] J. C. Ma and D. A. Dougherty, The Cation-π Interaction, Chem. Rev., 97 (1997) 1303-1324.

Figure 1. (Color online) (a) Device configuration of planar heterojunction perovskite solar cells. (b) The molecular structure of NPB. (c) and (d) DFT calculations for the two stable molecular structures of NPB-MA^+ with the lowest energies.

Figure 2. (Color online) Photovoltaic properties of perovskite films with and without NPB. (a) *J*-*V* curves of the champion PSCs with different concentration of NPB introduced into $MAPbI_3$. (b) IPCE curves and the integrated current curve of the PSCs. (c) Steady-state photocurrent and efficiency of PSCs with NPB. (d) Best *J*-*V* data in forward (FS) and reverse (RS) scans.

Figure 3. (Color online) (a) UV-visible absorption spectrum of (b) Photoluminescence spectra of perovskite films without and with NPB. (c) Nyquist plots of PSCs with and without NPB. The inset is the equivalent circuit model for fitting curves. (d) Dark *J*–*V* characteristics of the PSCs with and without NPB.

Figure 4. (Color online) X-ray diffraction (a) and top view SEM images (b-f) of perovskite films with different concentration of NPB introduced into $CH_3NH_3PbI_3$. The scale bar is 200 nm.

Figure 5. (Color online) (a) Stability of PSCs with and without NPB. These PSCs were measured every 24 h and stored in ambient air before and after *J*–*V* measurement. The inset is water contact angles of perovskite films with and without NPB on glass substrate. (b) XRD pattern were observed after the sample stored in air for 48 h.

(a)

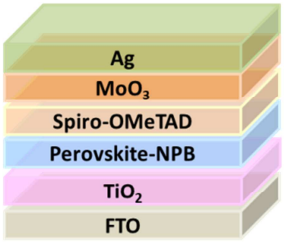

(b)

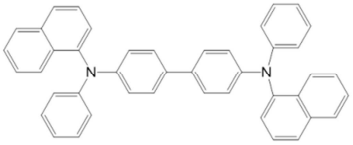

NPB

(c)

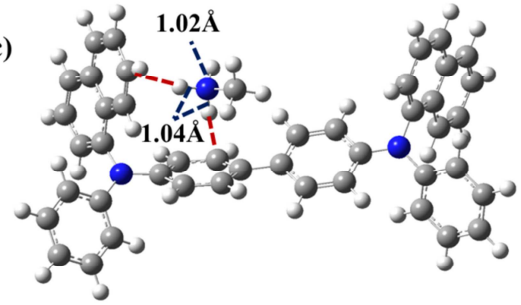

(d)

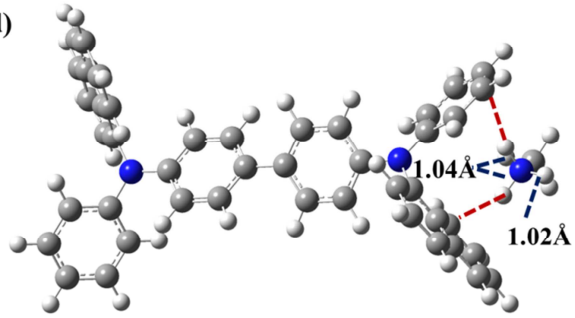

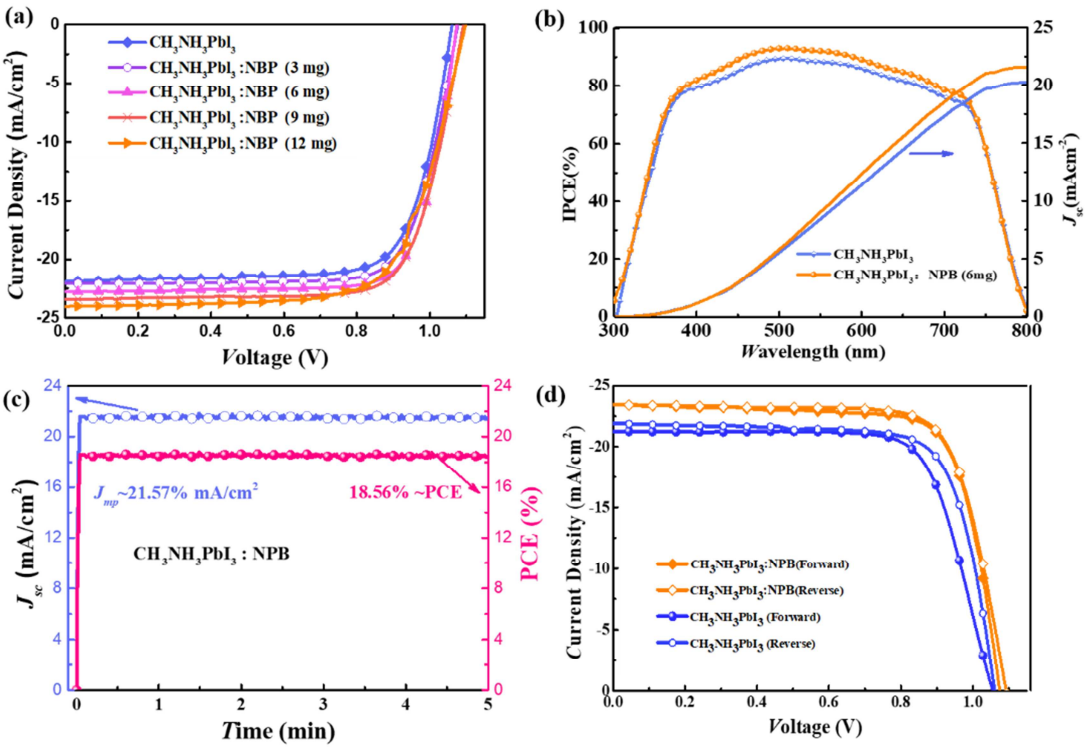
(a)
Current Density (mA/cm^2)
Voltage (V)
$CH_3NH_3PbI_3$
$CH_3NH_3PbI_3$:NBP (3 mg)
$CH_3NH_3PbI_3$:NBP (6 mg)
$CH_3NH_3PbI_3$:NBP (9 mg)
$CH_3NH_3PbI_3$:NBP (12 mg)
(b)
IPCE(%)
J_{sc} (mAcm^{-2})
Wavelength (nm)
$CH_3NH_3PbI_3$
$CH_3NH_3PbI_3$: NPB (6mg)
(c)
J_{sc} (mA/cm^2)
PCE (%)
Time (min)
J_{mp}~21.57% mA/cm^2
18.56% ~PCE
$CH_3NH_3PbI_3$: NPB
(d)
Current Density (mA/cm^2)
Voltage (V)
$CH_3NH_3PbI_3$:NPB(Forward)
$CH_3NH_3PbI_3$:NPB(Reverse)
$CH_3NH_3PbI_3$ (Forward)
$CH_3NH_3PbI_3$ (Reverse)

--

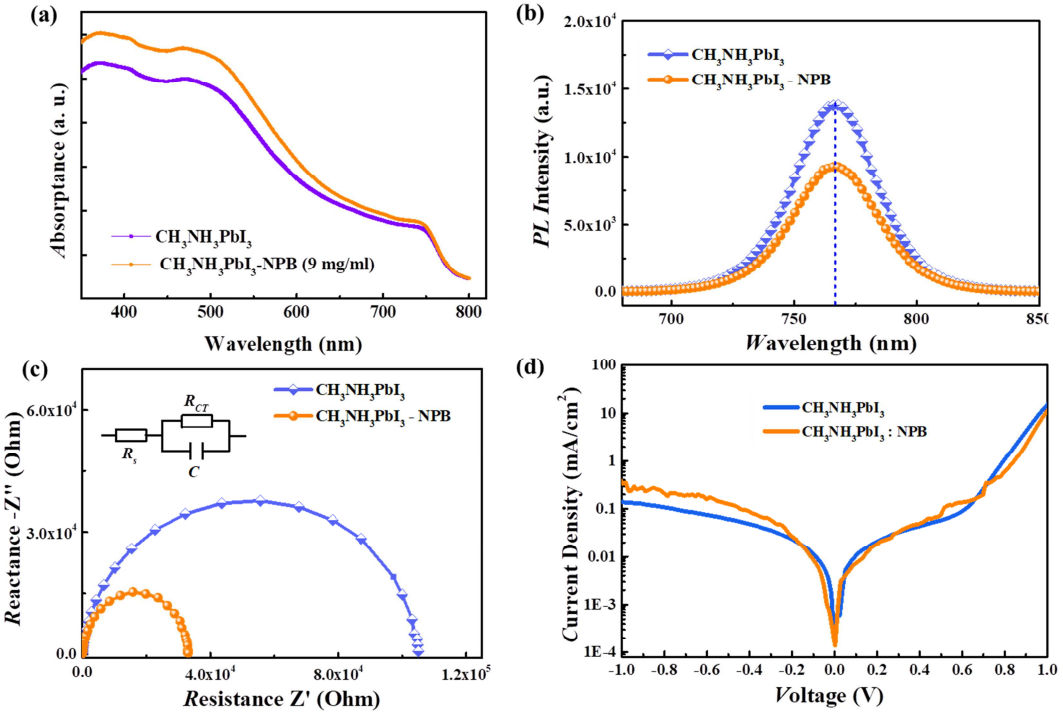
(a)
Absorptance (a. u.)
Wavelength (nm)
CH3NH3PbI3
CH3NH3PbI3-NPB (9 mg/ml)
(b)
PL Intensity (a.u.)
Wavelength (nm)
CH3NH3PbI3
CH3NH3PbI3 - NPB
(c)
Reactance -Z'' (Ohm)
Resistance Z' (Ohm)
RCT
Rs
C
CH3NH3PbI3
CH3NH3PbI3 - NPB
(d)
Current Density (mA/cm2)
Voltage (V)
CH3NH3PbI3
CH3NH3PbI3 : NPB

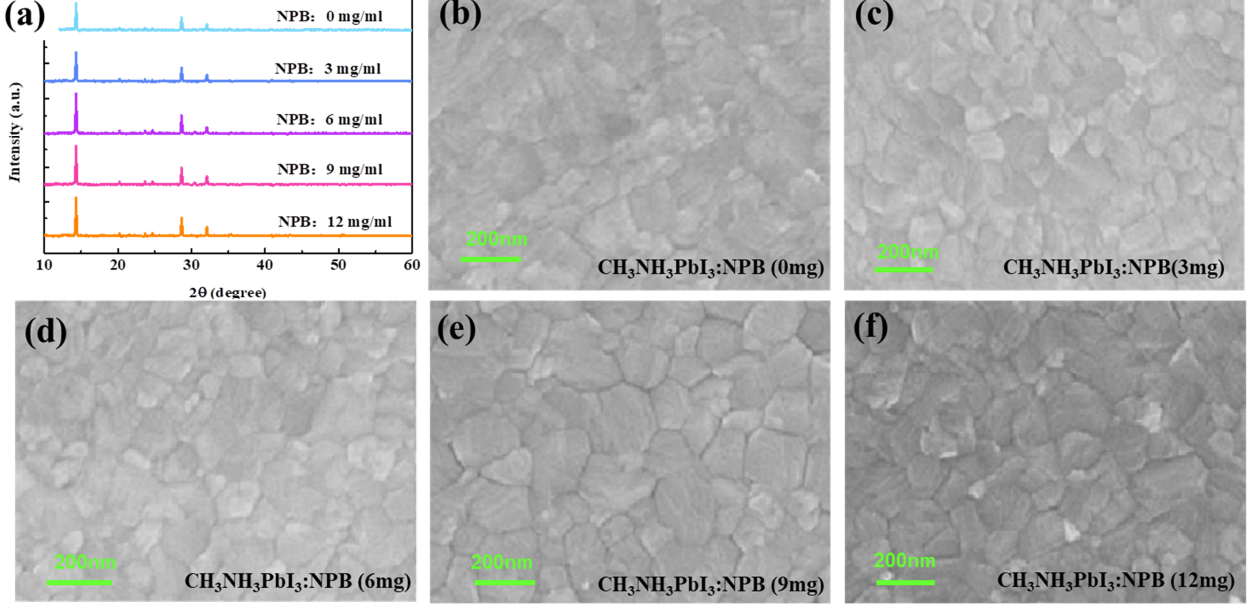
(a)
NPB: 0 mg/ml
NPB: 3 mg/ml
NPB: 6 mg/ml
NPB: 9 mg/ml
NPB: 12 mg/ml
Intensity (a.u.)
10
20
30
40
50
60
2θ (degree)
(b)
200nm
CH3NH3PbI3:NPB (0mg)
(c)
200nm
CH3NH3PbI3:NPB(3mg)
(d)
200nm
CH3NH3PbI3:NPB (6mg)
(e)
200nm
CH3NH3PbI3:NPB (9mg)
(f)
200nm
CH3NH3PbI3:NPB (12mg)

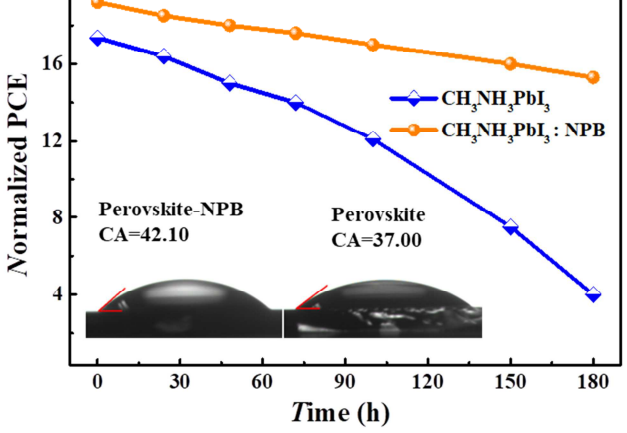

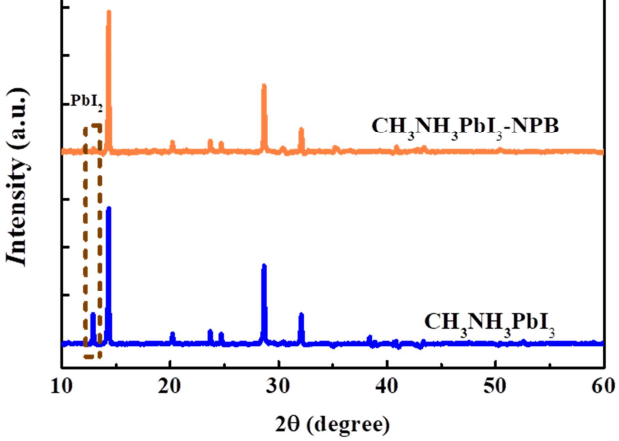

different concentrations of NBP introduced into $MAPbI_3$ as an active absorber layer.

Active layer with different concentration of NPB	V_{oc} (V)	J_{sc} (mA/cm^2)	FF (%)	PCE (%)
0 mg/ml NPB	1.07	21.93	74	17.36
3 mg/ml NPB	1.08	22.09	76	18.11
6 mg/ml NPB	1.08	22.80	77	18.90
9mg/ml NPB	1.09	23.42	75	19.22
12 mg/ml NPB	1.10	23.95	71	18.70

High Light

1. Carrier-recombination inhibition by the cation–π interaction in planar perovskite solar cells.
2. NPB was introduced into $CH_3NH_3PbI_3$ layer to form cation–π interaction.
3. An enhanced efficiency of 19.22% for the perovskite solar cells with negligible hysteresis are acquired.